New Journal of Physics
The open access journal at the forefront of physics

Deutsche Physikalische Gesellschaft DPG IOP Institute of Physics

PAPER • OPEN ACCESS

Quantum defect theory description of weakly bound levels and Feshbach resonances in LiRb

To cite this article: Jesús Pérez-Ríos *et al* 2015 *New J. Phys.* **17** 045021

New Journal of Physics
The open access journal at the forefront of physics

Deutsche Physikalische Gesellschaft DPG
IOP Institute of Physics

Published in partnership with: Deutsche Physikalische Gesellschaft and the Institute of Physics

CrossMark

OPEN ACCESS

RECEIVED
13 December 2014

REVISED
12 March 2015

ACCEPTED FOR PUBLICATION
20 March 2015

PUBLISHED
27 April 2015

PAPER

Quantum defect theory description of weakly bound levels and Feshbach resonances in LiRb

Jesús Pérez-Ríos[1], **Sourav Dutta**[2], **Yong P Chen**[1,3] **and Chris H Greene**[1]

[1] Department of Physics and Astronomy, Purdue University, 47907 West Lafayette, IN, USA
[2] Raman Research Institute, C. V. Raman Avenue, Sadashivanagar, Bangalore-560080, India
[3] School of Electrical and Computer Engineering, Purdue University, 47907 West Lafayette, IN, USA

E-mail: jperezri@purdue.edu

Keywords: quantum defect theory, frame transformation, Feshbach resonances, two-photon photoassociation

Abstract

The multichannel quantum defect theory (MQDT) in combination with the frame transformation (FT) approach is applied to model the Fano–Feshbach resonances measured for $^{7}Li^{87}Rb$ and $^{6}Li^{87}Rb$ Marzok *et al* (2009 *Phys. Rev.* A **79** 012717). The MQDT results show a level of accuracy comparable to that of previous models based on direct, fully numerical solutions of the the coupled channel Schrödinger equations. Here, energy levels deduced from 2-photon photoassociation (PA) spectra for $^{7}Li^{85}Rb$ are assigned by applying the MQDT approach, obtaining the bound state energies for the coupled channel problem. Our results confirm that MQDT yields a compact description of PA observables as well as the Fano–Feshbach resonance positions and widths.

1. Introduction

Ultracold molecules are currently generating tremendous interest in the atomic, molecular, and optical physics community due to their potential applications as valuable tests and extensions of our understanding of processes in chemical physics, few-body physics and fundamental physics. In particular, ultracold molecules are expected to enable precise control of chemical reactions [1–3], studies of novel quantum phase transitions [4–6], realizations of novel dynamics in low-energy collisions [7], and tests of the possible time variation of the fundamental constants of nature [8, 9]. Moreover, ultracold molecules could shed light on the fundamental laws and symmetries of nature, through measurements of the electric dipole moment of the electron [10–12]. These measurements have already been able to rule out some theories that were proposed as alternatives to the standard model.

Molecules can be brought down to the ultracold regime by either direct or indirect methods. Direct schemes employ external fields (electric fields for polar molecules, and magnetic fields for paramagnetic molecules), or sympathetic cooling via collisions with colder atoms that act as a dissipative medium for the molecules to move through. On the contrary, indirect methods start with an ensemble of ultracold atoms, and then external fields are used to glue the atoms together to form ultracold molecules. External magnetic field ramps have been used to create ultracold molecules by making use of Fano–Feshbach resonances associated with the atom–atom interaction [9], in the so-called magnetoassociation technique [13]. Laser fields can also provide useful interactions with ultracold molecules. A photon resonant with an excited atomic state can be absorbed while an ultracold atom collides with a ground state atom, in a photoassociation (PA) process [14]. After the absorption, the ultracold molecule in an excited state can decay to the ground state by spontaneous emission.

The effectiveness of indirect cooling techniques depends on details of the atom–atom interaction. For this reason, indirect cooling methods can be a useful probe of the atom–atom interaction potential. Indeed, the results coming from MA or PA can be used to calculate an accurate atom–atom interaction through quantum scattering theory. This theory is based on the numerical solution of the radial coupled Schrödinger equations out to a large distance where the asymptotic conditions are applied [15]. While accurate, this method can be computationally demanding due to the large number of channels that are frequently involved, and because the

scattering wave function requires propagation out to such long distances. In this respect, multichannel quantum defect theory (MQDT) can be an efficient alternative.

MQDT was born in atomic physics long ago, as a highly successful theory to explain the spectra of autoionizing states in complex atoms and the link between bound and continuum states of an outermost atomic electron [16–18]. Since those early developments, MQDT has been extended beyond the long-range Coulomb interaction to other long range potentials [19, 20]. In particular, it has been applied to conventional atomic collisions [21, 22], and ultracold atomic collision [23–28]. MQDT exploits the fact that at long-range the coupling between the channels is negligible, and this permits a systematic separation of short-range and long-range influences on the two-body physics. Specifically, for some long range potentials, an analytic solution of the scattering wave function can be found in terms of quantum defects that are almost energy independent. For other potentials it is advantageous to implement a numerical version of the long range QDT solutions, appropriately characterized in a way that makes the energy- and field-dependences of scattering observables as explicit as possible.

In some applications, MQDT is employed in an essentially exact manner, in that accurate solutions of the close-coupling equations are obtained out to a distance around $r_0 = 30$–50 a.u., and then matched to linear combinations of single channel solutions (f_i, g_i) in the appropriate long range potential for each channel i. In the present context, of course, those are van der Waals long range potentials in every channel. For other applications, a simpler 'frame transformation (FT) approximation' that we abbreviate as MQDT-FT is utilized, as an alternative to explicitly solving the coupled differential equations in the inner region $r < r_0$.

The approximate MQDT-FT treatment is the version utilized for the present study. A similar MQDT-FT approach was developed by Hanna *et al* [29]. The concept of the FT formulation is to start from single-channel values of the singlet and triplet s-wave scattering lengths, which include no Zeeman or hyperfine couplings. These give the phases of the wavefunction in those short-range scattering eigenchannels, and they can then be rotated through a unitary transformation matrix into the asymptotic representation in which the atomic energy levels have been diagonalized (with the internal and external magnetic couplings included). In some systems, accurate or approximate scattering lengths a_S, a_T are already known for the singlet and triplet symmetries of an alkali metal dimer, respectively. The phase information contained in those scattering lengths can be recast as two short-range eigen-quantum-defects, μ_S, μ_T which represent energy-analytic phaseshifts relative to the van der Waals (f, g), and which vary far more slowly with energy than the scattering lengths themselves.

After frame-transforming these short range eigen-quantum-defects into the hyperfine plus Zeeman representation, a full $N \times N$ smooth reaction matrix is obtained for the system, and after closed channel elimination, Fano–Feshbach resonances emerge at various energies and magnetic field strengths B. (The closed-channel elimination step simply imposes correct exponentially decaying boundary conditions in the energetically closed channels.) The present study adopts the conventions for single-channel long-range field solutions are chosen to be those introduced by Ruzic *et al* [27, 30]. They represent a particular standardization of the long-range (f, g), and there are four 'long-range QDT parameters' which are standard and reasonably simple in their energy dependence, and which embody the crucial energy-dependences and magnetic field dependences that are controlled by the van der Waals physics and the hyperfine plus Zeeman Hamiltonian. (There are minor differences between the standardizations introduced by [27] and those used in alternative variants of QDT (e.g. different from those of Burke *et al* [23] of Gao [31] or of Mies and Raoult [24]). The version used here for the simplified FT procedure is taken from Pires *et al* [28]. Our study here determines the short-range singlet and triplet quantum defects for two isotopologues ^{6}Li^{87}Rb and ^{7}Li^{87}Rb. The optimum values of the short-range quantum defects are chosen to be those that describe most accurately the position of the observed Fano–Feshbach resonances. In another application developed in the following, MQDT is applied to assign the lines observed in two-color PA spectra for ^{7}Li^{85}Rb. Finally, some concluding remarks will address the applicability of MQDT to spectroscopic processes in ultracold physics.

2. MQDT: bound state calculations

Details about MQDT can be found elsewhere [23, 27, 28, 30, 32]. Here only a brief description of the main features of the MQDT approach and its application to the calculation of bound states with coupled channels is presented.

For two-body collisions in the presence of an external magnetic field, the wave function can be expanded in the basis of N hyperfine plus Zeeman states (channels) that include the centrifugal angular momentum l_i

$$\Psi_i(R, \Omega) = \frac{1}{R}\sum_{i=1}^{N}\Phi(\Omega)\Psi_i(R), \tag{1}$$

where Ω represents all angular coordinates and spin degrees of freedom. Equation (1) must be a solution of the Schrödinger equation, leading to a set of coupled radial equations

$$\sum_{j=1}^{N}\left[\left(-\frac{\mathrm{d}^2}{\mathrm{d}R^2}+\frac{l_j\left(l_j+1\right)}{R^2}\right)\delta_{ij}+V_{ij}(R)\right]\Psi_j(R)=E_i\Psi_i(R). \tag{2}$$

The matrix $V_{ij}(R)$ accounts for the coupling between different channels due to the interaction potential between the colliding particles. E_i denotes the available kinetic energy for the ith channel and it is given by $E_i = E - E_i^{\mathrm{thres}}$, where E is the collision energy and E_i^{thres} stands for the Zeeman energy of the i channel.

All lengths are expressed in units of the characteristic length scale β associated to the potential V, and all energies are in units of the corresponding characteristic length scale $E_\beta = \frac{\hbar^2}{2\mu\beta^2}$, where μ is the reduced mass. The long-range behavior of V specifies β and hence E_β. In particular, the long-range interaction between two S-state atoms (such as two alkali atoms) leads to an isotropic van der Waals interaction $V = -C_6/R^6$, and the characteristic length is given by $\beta = (2\mu C_6/\hbar^2)^{1/4}$, denoted the van der Waals length and the corresponding energy scale is called van der Waals energy. In some references the van der Waals length is defined as $\beta/2$ [33].

For most two-body collisions involving neutral species the long-range tail of the potential is dominated by the van der Waals interaction. In such systems, the channels become approximately uncoupled beyond a radius R_M. In general, equation (2) has N independent solutions that satisfy the physical boundary conditions $\Psi_i = 0$ at $R = 0$. The N solutions of equation (2) can be regarded as the column vectors of the $N \times N$ solution matrix M. Thus, matching M to single-channel reference wave function (uncoupled) $\hat{f}$ and $\hat{g}$ in each channel beyond R_M defines the short-range reaction matrix K [32]

$$M_{ij}(R) = \hat{f}_i(R)\delta_{ij} - \hat{g}_i(R)K_{ij}^{\mathrm{sr}}. \tag{3}$$

In particular, $\hat{f}_i(R)$ and $\hat{g}_i(R)$ are the regular and irregular solutions of the uncoupled Schrödinger equations in the long-range potential V^{lr}

$$\left[-\frac{\mathrm{d}^2}{\mathrm{d}R^2}+\frac{l_i\left(l_i+1\right)}{R^2}+V_i^{\mathrm{lr}}(R)-E_i\right]\begin{pmatrix}\hat{f}_i(R)\\ \hat{g}_i(R)\end{pmatrix}=0. \tag{4}$$

The matrix K^{sr} encapsulates all the information about the short-range physics and channel coupling, whereas the standardized (smooth, analytic in energy) reference wave functions $\hat{f}_i(R)$ and $\hat{g}_i(R)$ describe the long-range physics. K^{sr} and the linearly independent reference wave functions contain all the information necessary to calculate the scattering observables, through the scattering matrix, S. The calculation of the S matrix requires two linearly independent, energy-normalized wave functions for open channels, and the bound-state wave function in each closed channel. As is standard in QDT, four long-range quantum defect parameters suffice to convert the smooth, short range reaction matrix K^{sr} into the physical S-matrix which depends strongly on energy and magnetic field strength. The present calculations are based on the standardization of the long-range QDT parameters defined in [27]. Two of the long range QDT parameters, namely A and $\mathcal{G}$, are used to generate a Wronskian-preserving transformation between the reference wave functions and two energy-normalized wave functions $f_i(R)$ and $g_i(R)$ in the open channels

$$\begin{pmatrix}f_i(R)\\ g_i(R)\end{pmatrix}=\begin{pmatrix}A_i^{1/2} & 0\\ A_i^{-1/2}\mathcal{G}_i & A_i^{-1/2}\end{pmatrix}\begin{pmatrix}\hat{f}_i(R)\\ \hat{g}_i(R)\end{pmatrix}. \tag{5}$$

The other long range QDT parameter at positive channel energy, η_i, represents for the asymptotic phase-shift of the energy-normalized f_i and g_i relative to the spherical Bessel functions. Finally, γ_i is the long range QDT parameter at negative energy that describes the phase-shift of the reference wave functions $\hat{f}_i$ and $\hat{g}_i$, relative to the exponentially growing and decay solutions asymptotically which characterize bound-state solutions. The formulas to calculate those long range QDT parameters are given elsewhere [27].

The MQDT parameters translate K^{sr} into observables. For a given collision energy E, some channels will be open whereas the remain will be closed. Both kind of channels are included in the K^{sr} matrix, which can be partitioned in terms of the open channel (P) and close channels (Q) contributions as

$$K^{\mathrm{sr}}=\begin{pmatrix}K_{PP}^{\mathrm{sr}} & K_{PQ}^{\mathrm{sr}}\\ K_{QP}^{\mathrm{sr}} & K_{QQ}^{\mathrm{sr}}\end{pmatrix}. \tag{6}$$

However, the presence of closed-channel components in the K^{sr} will lead to unphysical solutions at large distances, due to the presence of exponentially growing terms. This problem is removed by means of the MQDT step referred to as the 'elimination of closed channels' [23], after which the physical K-matrix is obtained from the formula:

$$K = K^{\rm sr}_{PP} - K^{\rm sr}_{PQ}\left(K^{\rm sr}_{QQ} + \cot\gamma\right)^{-1} K^{\rm sr}_{QP}. \tag{7}$$

This expression shows explicitly the potentially resonant influence of closed-channel pathways. The resulting K matrix has dimensions $N_P \times N_P$, with N_P the number of open channels at the given collision energy E. In particular, from equation (7) discrete bound states can be obtained as the roots of the following equation:

$$\det\left(K^{\rm sr}_{QQ} + \cot\gamma\right) = 0, \tag{8}$$

where $\cot\gamma$ represents a diagonal matrix in channel space whose elements are equal to the closed channel QDT parameter $\cot\gamma$.

2.1. FT machinery

MQDT assumes that the short-range reaction matrix $K^{\rm sr}$ depends very weakly on energy. Therefore, it can be calculated at just a few energies and then be interpolated between these values. In some cases, a single evaluated $K^{\rm sr}$ matrix for a single chosen energy (usually close to the threshold) at zero magnetic field can be utilized to describe the scattering observables over a wide range of energies and magnetic fields.

Generally, in scattering problems there is a representation where the Hamiltonian is diagonal at short-range and another one where the same Hamiltonian is diagonal at long-range. This difference in representations because the terms in the Hamiltonian that dominate at small distance often fail to commute with the terms dominant at large distance. The FT technique relies on an energy independent unitary transformation between the two representations. The MQDT-FT technique has been successfully applied to ultracold atomic collisions in the presence of an external magnetic field [23, 34, 35]. We follow here the method employed in a very recent study of the Li-Cs heteronuclear system [28].

At short-range, due to the dominant role of the exchange energy, the collisional eigenstates are represented as $|\alpha\rangle \equiv |(s_A s_B) S\left(i_A i_B\right) I\ FM_F\rangle$, s_i denotes the electronic spin of the ith atom, i_i stands for the nuclear spin of the ith atom, F is the total angular momentum of the molecule and M_F is its projection on the quantization axes. In this basis the $K^{\rm sr}$ matrix is diagonal and reads as:

$$K^{\rm sr}_{\alpha\alpha} = \tan\left(\pi\mu_\alpha\right)\delta_{\alpha\alpha}, \tag{9}$$

where μ_α denotes the short-range single-channel quantum defects for the singlet μ_S and triplet μ_T states, which are approximated throughout this study as being energy independent and magnetic field independent.

For the long-range part of the Hamiltonian, the hyperfine plus Zeeman energy is the dominant term of the Hamiltonian, and hence the collisional channels will be represented in the basis of the hyperfine+Zeeman eigenstates $|i\rangle = |m_A z_A,\ m_B z_B\rangle$, which are a linear combination of the basis set $|f_A m_A,\ f_B m_B\rangle$, whose superposition coefficients are functions of the magnetic field. The MQDT-FT method utilizes the energy independent unitary transformation between the short-range basis set $|\alpha\rangle$ and the long-range basis set $|i\rangle$, which is given by standard angular momentum coefficients (Clebsch–Gordan and Wigner 9-j coefficients) and the Breit–Rabi eigenvectors, and we denote these transformation matrix elements as $\langle z_A z_b\ |f_A f_B\rangle^{(m_A,m_B)}$, etc, and they are computed as

$$\begin{aligned} U_{i,\alpha} = \sum_{f_A f_B f} &\left\langle z_A,\ z_B\ \middle|f_A,\ f_B\right\rangle^{(m_A,m_B)} \left\langle f_A m_A,\ f_B m_B\ |FM_F\right\rangle \\ &\times \left\langle \left(s_A i_A\right) f_A \left(s_B i_B\right) f_B \middle| (s_A s_B) S\left(i_A i_B\right) I\right\rangle^{(F)}. \end{aligned} \tag{10}$$

The short-range reaction matrix is approximated here as being exactly diagonal in the short-range basis set, whereas the scattering observables are defined in the long-range basis set (hyperfine + Zeeman). Angular momentum coupling theory ensures the existence of the unitary transformation matrix connecting these two representations via equation (10), and therefore the smooth, short-range reaction matrix is given to an excellent approximation by:

$$K^{\rm sr}_{ij} = \sum_\alpha U_{i,\alpha} K^{\rm sr}_\alpha U^T_{\alpha,j}, \tag{11}$$

where T denotes the matrix transpose. Note that l, the quantum number associated with the centrifugal angular momentum does not appear in equation (10), therefore the FT does not involve couplings between the atomic degrees of freedom (spin, nuclear spin, angular momentum) and the collisional degree of freedom. In systems where magnetic dipole–dipole or quadrupole interactions are important, it could be desirable to include off-diagonal coupling terms in l, but those are often sufficiently weak that they can be treated perturbatively. The short-range quantum defects $\mu^{\rm sr}$ do depend on l, but most of that l-dependence is known analytically; a small l-dependent correction can be applied as in [28].

Table 1. Comparison of the resulting ^{6}Li^{87}Rb and ^{7}Li^{87}Rb Fano–Feshbach resonance positions from MQDT and CC methods to the observed resonances. A van der Waals $C_6 = 2550$ a.u. has been employed for the MQDT calculations (see text for details). The experimentally observed positions $B_0^{\rm exp}$ and widths $\Delta B^{\rm exp}$ are taken from [37]. The resonance positions and widths calculated by the MQDT approach are denoted by $B_0^{\rm MQDT}$ and $\Delta B^{\rm MQDT}$, respectively. The resonances positions based on the CC approach $B_0^{\rm CC}$ and widths $\Delta B^{\rm CC}$ are taken from the model I of [37]. The positions and widths of the resonances are given in Gauss. The nature of the resonances is shown in the last column of the table, $l = 0$ and $l = 1$ represent s-wave and p-wave respectively. The weighted rms deviation $\delta B^{\rm rms}$ (see text for details) is also shown.

Open channel	$B_0^{\rm exp}$ (G)	$\Delta B^{\rm exp}(G)$	$B_0^{\rm MQDT}(G)$	$\Delta B^{\rm MQDT}(G)$	$B_0^{\rm CC}(G)$	$\Delta B^{\rm CC}(G)$	l
^{6}Li $\lvert\frac{1}{2}, \frac{1}{2}\rangle + {}^{87}$Rb $\lvert 1, 1\rangle$	882.02	1.27	882.75		882.42		1
	1066.92	10.62	1067.05	6.26	1066.92	7.4	0
^{7}Li $\lvert 1, 1\rangle + {}^{87}$Rb $\lvert 1, 1\rangle$	389.5	0.9	390.69		390.2		1
	447.4	1.1	446.83		445.6		1
	565	6	563.19	7.8	568.8	7.9	0
	649	70	653.09	204	650.6	175	0
$\delta B^{\rm rms}$ (G)			0.67		1.02		

3. Analyzing Feshbach resonances for LiRb

The MQDT-FT approach as presented in the previous section is applied here to describe Fano–Feshbach resonances in LiRb. In particular, we will focus on ^{6}Li^{87}Rb and ^{7}Li^{87}Rb, two isotopic mixtures for which Feshbach resonances have been experimentally observed [36, 37]. Feshbach resonances have been observed and characterized in other isotopic mixtures [38, 39], as well as detailed studies of the PA prospects for LiRb have been carried out recently [40].

The MQDT-FT has been implemented by using the long-range potentials reported in [37], most importantly the long-range C_6 coefficient is 2550 a.u. This value corresponds to the model I of [37]. The short-range physics is fully characterized by means of the field independent and energy independent quantum defects μ_S and μ_T, through the short-range reaction matrix. These short-range quantum defects are adjusted to find an optimal agreement between the predicted position and width of the Fano–Feshbach resonances. The FT technique is used to transform the short-range reaction matrix (see equation (11)) into the long-range basis (hyperfine + Zeeman states). Finally, four long range QDT parameters in each channel that depend on the channel energy are needed for establishing a relationship between the short-range and long-range physics, where the asymptotic conditions are applied. The present study uses these parameters, denoted as $\mathcal{G}$, A, η and γ, which have been determined once and for all for a pure van der Waals potential at long range $-C_6/R^6$ [27, 28, 30]. The long-range quantum defects are standard and can be used for any alkali–alkali collision. They have been tabulated as functions of a single dimensionless variable which is the product of the van der Waals length and the wave number k [27, 28]. Finally, by means of equation (8), the magnetic field locations of the low energy Fano–Feshbach resonances are calculated. This procedure yields the resonance as positions, as functions of the short-range quantum defects. The short-range quantum defects, μ_S and μ_T may be regarded as fitting parameters to predict the positions of all resonances observed experimentally. In addition, the MQDT-FT approach also enables the computation of scattering total and partial cross sections, through the very well-known relation between the K-matrix (equation (6)) and the S-matrix (see e.g. [15]).

The MQDT-FT results for ^{7}Li^{87}Rb and ^{6}Li^{87}Rb, using the hyperfine constants reported in [41], in comparison with the CC calculations from [37] are shown in table 1. Parenthetically, the MQDT-FT calculation reported here neglects entirely the spin–spin and second-order spin–orbit interactions. The fitting of the short-range quantum defects (μ_S and μ_T) is performed by taking into account the s-wave as well as the p-wave Fano–Feshbach resonances. In addition, the fitting is performed separately for each different isotopic mixture under study, without making use of any mass-scaling argument. For the fitting, three independent fitting parameters are employed [28], these are small deviation from the initial short-range quantum defects coming from the long-range potential of the model I of Marzok *et al* [37]. For the MQDT calculation a collision energy of 8 μK has been assumed. The quality of the results are measured by means of the weighted root mean square (rms) deviation $\delta B^{\rm rms}$ on the resonance position, which is defined as

$$\delta B^{\rm rms} = \sqrt{\frac{\sum_{i=1}^{N} \delta_i^2 \delta B_i^{-2}/N}{\sum_{i=1}^{N} \delta B_i^{-2}}}. \tag{12}$$

The summation is performed over N Fano–Feshbach resonances for a given isotopic mixture, δB_i denotes the experimental uncertainty of the resonance positions and $\delta_i = B_0^{\rm model} - B_0^{\rm exp}$, where model stands for MQDT-FT and CC, whereas the superscript exp denotes the experimental resonance positions. Table 1 shows that the MQDT-FT approach gives agreement with the position of measured resonances comparable to that achieved in previous CC calculations [37], which are far more computationally demanding. Indeed the weighted rms

Table 2. Calculated *s*-wave and *p*-wave short-range quantum defects and scattering lengths (only for the *s*-wave) for the uncoupled singlet (S) and triplet (T) states of different isotopic mixtures of LiRb molecule. The scattering length is given in units of the Bohr radius (a_0).

	s-wave				*p*-wave	
Molecule	μ_S	μ_T	$a_S\,(a_0)$	$a_T\,(a_0)$	μ_S	μ_T
^{6}Li^{87}Rb	0.2572	0.3184	−1.87	-22.70	0.0045	0.0648
^{7}Li^{87}Rb	−0.0817	0.3845	53.20	−68.85	−0.3282	0.1380
^{7}Li^{85}Rb	−0.1259	0.3707	59.73	−55.49	−0.3724	0.1242

deviation is smaller for the MQDT-FT results than for CC ones. Positions of the Fano–Feshbach resonances can be inferred from the divergences of the computed scattering length versus the magnetic field.

The widths of the *s*-wave Feshbach resonances shown in table 1 for the MQDT approach have been obtained by first calculating the scattering length as a function of the external magnetic field. Next, the scattering length is fitted by means of the function $a\,(B) = a_{\rm bg}\left(1 + \sum_{i=1}^{N} \Delta B_i/(B - B_i)\right)$. Here B_i denotes the position of the Feshbach resonance, ΔB_i represents the width of the resonance, and the background scattering length $a_{\rm bg}$ is a global parameter for the fitting. The MQDT results for the width of the *s*-wave resonance of ^{6}Li^{87}Rb is in good agreement with the experimental reported data [37]. On the contrary, the width of the Feshbach resonances associated with ^{7}Li$\,|1,\ 1\rangle + {}^{87}Rb\,|1,\ 1\rangle$ are larger than the reported experimental values. A similar trend is observed for the CC calculations, even for other isotopic mixtures of LiRb [38, 39]. It seems that all the theoretical predictions overestimate the width of the Feshbach resonances for LiRb.

The optimal short-range quantum defects, as well as the scattering lengths extracted from them, are shown in table 2. In addition, the *p*-wave short-range quantum defects are also shown in the same table for all the isotopologues for LiRb studied in this work. The scattering length calculated by the MQDT-FT compares well with the previously reported CC calculation [37], showing that MQDT can accurately predict such Fano–Feshbach resonance positions.

4. Two-photon PA: analysis of the least bound states of ^{7}Li ^{85}Rb

Feshbach resonances have not been observed to date for the ^{7}Li - ^{85}Rb system. However, we have recently measured the least bound states of ^{7}Li ^{85}Rb using Raman-type two-photon PA, the experimental details of which will be described elsewhere [42].

For shallow bound states, the associated wave functions mainly sample the long-range tail of the potential. In such a system, the MQDT approach becomes a valuable tool for the calculation of such bound states. For Li–Rb, ground state collisions can occur in any of the two distinct potentials, $X^1\Sigma^+$ and $a^3\Sigma^+$. Both potentials will be coupled due to the presence of hyperfine interaction in both atoms. The MQDT approach naturally includes such coupling between the singlet and triplet potentials through their respective quantum defects μ_S and μ_T (see equation (9)) and of course the hyperfine plus Zeeman terms in the Hamiltonian which do not commute with the total spin operators. For these calculations the hyperfine constants of [41] have been used, and for the calculation of the quantum defects, the singlet and triplet scattering lengths reported in [37] have been utilized. The long-range coefficients of the previous section have been employed here as well. The $B = 0$ binding energies for the *s* and *p*-wave bound states calculated using the MQDT-FT approach are listed in table 3. Those bound states have been obtained through the short-range quantum defects listed in table 2. The quantum defects have been obtained from the calculated scattering length reported by Marzok *et al* [37], and fitted a posteriori, as it is explained in the previous section. In particular, we have employed the same fitting parameters that were obtained for the fitting of ^{7}Li^{87}Rb, since the isotopic effect of Rb should be very small in comparison with the case at hand. In table 3 it is shown the total F, the total molecular angular momentum (including the hyperfine structure), associated to each state. The F quantum number has been calculated by means a block diagonal procedure, i.e., by varying the number of channels taken into account for the calculations of bound states. In each step, a new block of channels associated to a given F were included, and hence revealing the nature of each bound state.

The scheme for Raman-type two-photon PA is shown in figure 1. The ultracold Li and Rb atoms in a dual species magneto-optical trap (MOT) collide predominantly in the Li (2s, $f_{\rm Li} = 2$) + Rb (5s, $f_{\rm Rb} = 2$) channel [43–45]. They are photoassociated, using a PA laser at frequency $\nu_{\rm PA}$, to form weakly bound electronically excited LiRb* molecules in a rovibrational level denoted by ν' from which they spontaneously decay to the electronic ground state or to free atoms leading to loss of atoms from the MOT [44, 45]. This loss of atoms is detected as a decrease in the fluorescence of the Li MOT. A second laser, called the Raman laser with frequency ν_R, is scanned across a bound-bound $\nu' \leftrightarrow \nu''$ transition between the electronically excited and ground states. The polarization

Table 3. *s*-wave and *p*-wave bound states binding energies (in GHz) calculated using the MQDT-FT approach. In the first column the total *F* for each bound state is shown (ignoring orbital angular momentum). The binding energies are referred to the threshold shown in the first row of the table.

(f_{Li}, f_{Rb})	(1, 2)	(2, 2)	(1, 3)	(2, 3)	(1, 2)	(2, 2)	(1, 3)	(2, 3)
	s-wave				*p*-wave			
F								
1	−1.67	−0.86	1.37	2.17	−3.37	−2.57	−0.34	0.46
2	−1.58	−0.77	1.45	2.26	−3.25	−2.45	−0.21	0.59
3	−1.44	−0.64	1.59	2.40	−3.00	−2.20	0.03	0.83
4		−0.43	1.80	2.61		−2.02	0.21	1.01
5				4.03				3.38
4		1.22	3.46	4.26		0.66	2.89	3.70
3	0.63	1.43	3.67	4.47	0.08	0.89	3.12	3.92
2	0.77	1.58	3.81	4.61	0.24	1.05	3.28	4.08
4		5.08	7.31	8.11		4.61	6.84	7.64
3	4.40	5.21	7.45	8.25	3.94	4.75	6.98	7.78
2	4.53	5.34	7.57	8.37	4.08	4.88	7.11	7.92
1	4.64	5.44	7.68	8.48	4.18	4.98	7.22	8.02
0	6.12	6.93	9.16	9.96	5.61	6.42	8.65	9.45
1	6.22	7.03	9.26	10.06	5.71	6.52	8.75	9.55
2	6.40	7.21	9.44	10.24	5.89	6.70	8.93	9.73
3	6.64	7.45	9.68	10.48	6.13	6.93	9.17	9.97

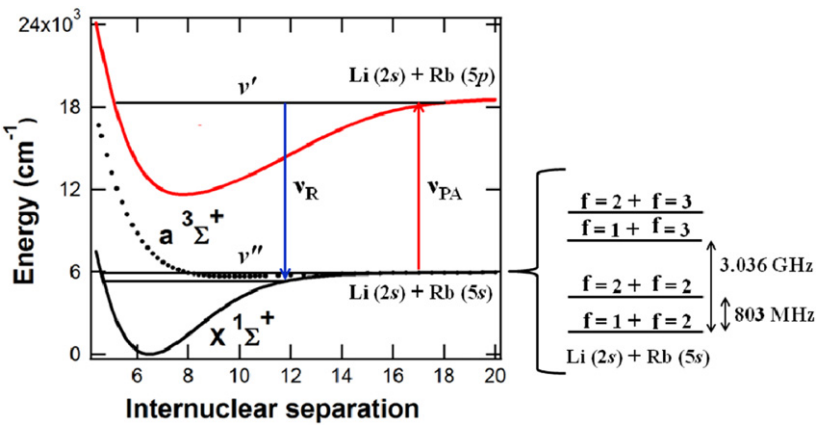

Figure 1. Scheme used for Raman type 2-photon spectroscopy for $^{7}Li^{85}Rb$. The inset to the right shows the different hyperfine channels along which the ground electronic state dissociates asymptotically. See text for details.

of the Raman laser is perpendicular to the polarization of the PA laser. When the Raman laser is resonant with the $\nu' \leftrightarrow \nu''$ transition it causes an Autler–Townes splitting in the ν' level leading to the PA laser going out of resonance [46], hence suppressing the PA induced atom loss. This suppression of atom loss is a signature of a Raman resonance and the binding energy of the ν'' level is given by $\Delta\nu = \nu_R - \nu_{PA}$. The uncertain in the experimental energies of the bound states is 60 MHz in relation with the accuracy of the wavelength-meter employed in the measurements.

In our experimental set up the linear polarizations of the lasers are perpendicular to each other, leading to a new set of selection rules. In particular, since Li and Rb are colliding predominantly through the *s*-wave initially, this implies that only *s*- and *d*-wave bound states will be allowed following the Raman process. For this reason, only the *s*-wave bound states have been considered for the assignment of the observed 2-photon PA lines, as are shown in table 4. In the same table are shown the experimentally observed 2-photon PA lines up to 3 GHz of binding energy.

There are two distinct potentials, $X^1\Sigma^+$ and $a^3\Sigma^+$, at small internuclear separations but at large internuclear separations both potentials approach the Li (2s) + Rb (5s) asymptote with the same C_6 coefficient. The bound states measured in our experiments are very close to the dissociation limit where the two potentials can be described with a single C_6 coefficient, and it is also the region for which the MQDT approach is expected to give

Table 4. Experimentally measured binding energies for s-wave bound states. The binding energies (in GHz) are represented in each column for each possible channel: Li (2s, $f_{Li} = 2$) + Rb (5s, $f_{Rb} = 2$), Li (2s, $f_{Li} = 1$) + Rb (5s, $f_{Rb} = 2$), Li (2s, $f_{Li} = 1$) + Rb (5s, $f_{Rb} = 3$) and Li (2s, $f_{Li} = 2$) + Rb (5s, $f_{Rb} = 3$), from left to right, respectively. The experimental uncertain for the bound states energies is 0.06 GHz (see text for details), not shown in the table for clarity. By comparing these energies with the MQDT values shown in table 3, tentative assignments are made and shown in the last column. The theoretical prediction for the bound states energies based on the MQDT approach are shown in parenthesis.

Name	(f_{Li}, f_{Rb}) (2, 2)	(f_{Li}, f_{Rb}) (1, 2)	(f_{Li}, f_{Rb}) (1, 3)	(f_{Li}, f_{Rb}) (2, 3)	Assignment
α	−0.63 (−0.64)	−1.43	1.61	2.41	$(f_{Li} = 2, f_{Rb} = 2), F = 3$
β	−0.31	−1.11	1.93	2.73 (2.61)	$(f_{Li} = 2, f_{Rb} = 3), F = 4$
γ	0.98	0.18	3.22	4.02 (4.03)	$(f_{Li} = 2, f_{Rb} = 3), F = 5$
δ	1.26 (1.22)	0.46	3.5	4.3	$(f_{Li} = 2, f_{Rb} = 2), F = 4$
ϵ	1.55 (1.58)	0.75	3.79	4.59	$(f_{Li} = 2, f_{Rb} = 2), F = 2$

reliable results. Since Li (2s) and Rb (5s) atoms have hyperfine structure, for $B = 0$ the electronic potentials at very large internuclear separation must dissociate along one of the four hyperfine channels: Li (2s, $f_{Li} = 1$) + Rb (5s, $f_{Rb} = 2$), Li (2s, $f_{Li} = 2$) + Rb (5s, $f_{Rb} = 2$), Li (2s, $f_{Li} = 1$) + Rb (5s, $f_{Rb} = 3$) or Li (2s, $f_{Li} = 2$) + Rb (5s, $f_{Rb} = 3$). Since we start with atoms colliding along the Li (2s, $f_{Li} = 2$) + Rb (5s, $f_{Rb} = 2$) channel all bound levels corresponding to this channel will have positive values for $\Delta\nu$. The same is true for the potential dissociation along the Li (2s, $f_{Li} = 1$) + Rb (5s, $f_{Rb} = 2$) hyperfine channel. Negative values $\Delta\nu$ necessarily have to be bound levels of the potentials dissociating along the Li (2s, $f_{Li} = 1$) + Rb (5s, $f_{Rb} = 3$) or the Li (2s, $f_{Li} = 2$) + Rb (5s, $f_{Rb} = 3$) hyperfine channels. In our case the binding energies are measured with respect to the Li (2s, $f_{Li} = 2$) + Rb (5s, $f_{Rb} = 2$) channel, so the relevant atomic hyperfine energy needs to be added or subtracted in order to calculate the binding energy measured with respect to different channels. To calculate the binding energy with respect to Li (2s, $f_{Li} = 1$) + Rb (5s, $f_{Rb} = 2$) channel we subtract 0.803 GHz (the Li hyperfine splitting), to calculate the binding energy with respect to the Li (2s, $f_{Li} = 1$) + Rb (5s, $f_{Rb} = 3$) channel we add 2.237 GHz (the difference between Rb and Li hyperfine splitting) and to calculate the binding energy with respect to the channel Li (2s, $f_{Li} = 2$) + Rb (5s, $f_{Rb} = 3$), we add 3.04 GHz (the Rb hyperfine splitting) to the observed values of $\Delta\nu$ (see table 4).

Finally, some discussion in relation with the assignments of the observed levels is pertinent. The presented assignment shown in table 4 have been done by comparing the observed position of the peaks and the predicted bound state energies (table 3). Deeper bound states have been observed in the current experiment, however they are not correctly described by the present approach, and their assignment cannot be performed. Since these states are deeper that the previous one, they could be explore part of the interaction potential that needs to be described beyond the C_6 coefficient, and therefore the approach presented will not be accurate enough. Another reason would be that those states are associated to *d*-wave bound states, and these are beyond the approach presented.

5. Summary and conclusions

The MQDT approach has been employed in two very different scenarios: Fano–Feshbach resonance description, and assignment of the 2-photon PA spectra. MQDT in addition with the FT has been employed to fit the observed experimental positions of the Fano–Feshbach resonances for $^7Li^{87}Rb$ and $^6Li^{87}Rb$. The *s*-wave quantum defects associated with the triplet and singlet potentials are used as the fitting parameters. Then the scattering lengths for triplet and singlet potentials have been obtained through the obtained quantum defects. The resulting fit using MQDT turns out to be as accurate as one obtains by solving the coupled-channel Schrödinger equation, but with much less numerical effort.

For 2-photon PA spectroscopy, MQDT is an excellent tool for the assignments of the observed spectra. The capability of MQDT for calculating shallow bound states (dominant by the long-range tail of the interaction) between coupled electronic states has been exploited. An outcome of this work is the assignments of our experimentally observed 2-photon PA lines. MQDT may also used for calculating the scattering length associated with the triplet and singlet electronic potentials, similar to our analysis of the Fano–Feshbach resonances. This is something that will be addressed in a subsequent publication.

Acknowledgments

This work has been supported in part by the AFOSR-MURI program, and in part by NSF under grand number PHY-130690. S Dutta acknowledge the Bilsland fellowship and YP Chen to OVPR incentivegrant from Purdue

University. We thank Brandon Ruzic for providing access to unpublished programs and data used in the MQDT calculations.

References

[1] Krems R V 2008 *Phys. Chem. Chem. Phys.* **10** 4079
[2] Krems R V 2005 *Int. Rev. Phys. Chem.* **24** 99
[3] Hudson E R, Ticknor C, Sawyer B C, Taatjes C A, Lewandowski H J, Bochiniski J R, Bohn J L and Ye J 2006a *Phys. Rev.* A **73** 063404
[4] Yi S and You L 2000 *Phys. Rev.* A **61** 041604
[5] Goral K, Santos L and Lewenstein M 2002 *Phys. Rev. Lett.* **88** 170406
[6] Santos L, Shlyapnikov G V and Lewenstein M 2003 *Phys. Phys. Lett.* **90** 250403
[7] Avdeenkov A V and Bohn J L 2003 *Phys. Rev. Lett.* **90** 043006
[8] Hudson E R, Lewandowski H J, Sawyer B C and Ye J 2006b *Phys. Rev. Lett.* **96** 143004
[9] Chin C and Flambaum V V 2009 *New J. Phys.* **11** 055048
[10] Hudson J J, Sauer B E, Tarbutt M R and Hinds E A 2002 *Phys. Rev. Lett.* **89** 023003
[11] Hudson J J, Kara D M, Smallman I J, Sauer B E, Tarbutt M R and Hinds E A 2011 *Nature* **473** 493
[12] The ACME Collaboration 2014 *Science* **343** 269
[13] Köhler T, Góral K and Julienne P S 2006 *Rev. Mod. Phys.* **78** 1311
[14] Jones K M, Tiesinga E, Lett P D and Julienne P S 2006 *Rev. Mod. Phys.* **78** 483
[15] Mott N F and Massey H 1965 *The Theory of Atomic Collisions* (New York: Oxford University Press)
[16] Schrödinger E 1921 *Z. Phys.* **4** 347
[17] Seaton M J 1966 *Proc. Phys. Soc.* **88** 801
[18] Fano U and Rau A R P 1986 *Atomic Collisions and Spectra* (Orlando, FL: Academic)
[19] Greene C H, Fano U and Strinati G 1979 *Phys. Rev.* A **19** 1485
[20] Greene C H, Rau A R P and Fano U 1982 *Phys. Rev.* A **26** 2441
[21] Mies F H 1984 *J. Chem. Phys.* **80** 2514
[22] Fourré I and Raoult M 1999 *J. Chem. Phys.* **101** 9709
[23] Burke J P, Greene C H and Bohn J L 1998 *Phys. Rev. Lett.* **81** 3355
[24] Mies F H and Raoult M 2000 *Phys. Rev.* A **62** 012708
[25] Raoult M and Mies F H 2004 *Phys. Rev.* A **70** 012710
[26] Croft J F E, Wallis O G, Hutson J M and Julienne P S 2011 *Phys. Rev.* A **84** 042703
[27] Ruzic B P, Greene C H and Bohn J L 2013 *Phys. Rev.* A **87** 032706
[28] Pires R, Repp M, Ulmanis J, Kuhnle E D, Weidemüller M, Tiecke T G, Greene C H, Ruzic B P, Bohn J L and Tiemann E 2014 *Phys. Rev.* A **90** 012710
[29] Hanna T M, Tiesinga E and Julienne P S 2009 *Phys. Rev.* A **79** 040701(R)
[30] www.physics.purdue.edu/fermion/Research/NJP2015qdt/
[31] Gao B 1998 *Phys. Rev.* A **58** 1728
[32] Aymar M, Greene C H and Luc-Koenig E 1996 *Rev. Mod. Phys.* **68** 1015
[33] Chin C, Grimm R, Julienne P S and Tiesinga E 2010 *Rev. Mod. Phys.* **82** 1225
[34] Burke J P 1999 *PhD Thesis* University of Colorado
[35] Gao B, Tiesinga E, Williams C J and Julienne P S 2005 *Phys. Rev.* A **72** 042719
[36] Deh C, Marzok C, Zimmermann C and Courteille P W 2008 *Phys. Rev.* A **77** 010701
[37] Marzok C, Deh C, Zimmermann C, Courteille P W, Tiemann E, Vanne Y V and Saenz A 2009 *Phys. Rev.* A **79** 012717
[38] Li Z, Singh S, Tscherbul T V and Madison K W 2008 *Phys. Rev.* A **78** 022710
[39] Li Z and Madison K W 2009 *Phys. Rev.* A **79** 042711
[40] Gacesa M, Ghosal S, Byrd J N and Côté R 2013 *Phys. Rev.* A **88** 063418
[41] Arimondo E, Inguscio M and Violino P 1977 *Rev. Mod. Phys.* **49** 31
[42] S Dutta, J Pérez-Ríos, D S Elliott, Y P Chen and C H Greene to be published
[43] Dutta S, Altaf A, Lorenz J, Elliott D S and Chen Y P 2014a *J. Phys.* B **47** 105301
[44] Dutta S, Elliott D S and Chen Y P 2013 *Europhys. Lett.* **104** 63001
[45] Dutta S, Lorenz J, Altaf A, Elliott D S and Chen Y P 2014b *Phys. Rev.* A **89** 020702(R)
[46] Abraham E R I, McAlexander W I, Sackett C A and Hulet R G 1995 *Phys. Rev. Lett.* **74** 1315